

## Structural and Dielectric Properties of $\text{La}^{3+}/\text{Mn}^{4+}$ Modified Lead Titanate Nanoceramics \*

Archana Shukla and R. N. P Choudhary

Department of Physics and Meteorology

IIT Kharagpur-721302, India

E-mail: [archana@phy.iitkgp.ernet.in](mailto:archana@phy.iitkgp.ernet.in)

(Received February 10, 2010)

**Abstract:** The nanocrystalline samples of  $\text{Pb}_{0.94}\text{La}_{0.06}\text{Mn}_x\text{Ti}_{1-x}\text{O}_3$  (PLMT) ( $x = 0, 0.04, 0.07, 0.10$ ) were prepared by using a novel mechanical activation followed by a conventional solid-state reaction technique. The calcination and sintering temperatures were optimized by thermal gravimetric analysis and repeated firing. Phase analysis using high resolution X-ray diffraction technique at room temperature suggests that compounds are formed in a single phase with tetragonal crystal system. The field effect scanning electron microscopy (FESEM) shows that materials have well-defined granular microstructures, separated by the grain boundaries. Measurement of dielectric properties (dielectric constant and dielectric loss) as a function of frequency and temperature were realized in PLMT ceramics. It shows a shift in the transition temperature towards the lower-temperature side with  $\text{La}^{3+}/\text{Mn}^{4+}$  substitution. The electrical conductivity calculated from impedance data has been observed to increase as a function of Mn concentration. The ac conductivity spectrum analysis suggests hopping of charge carriers among localized site as the possible mechanism for electrical conduction.

**Key words:** Nanoceramics; Microstructure; Dielectric constant; Dielectric loss; Conductivity.

### 1. Introduction

For a long time, ferroelectric materials have been exploited as one of the most promising class of materials to be used for electronic devices with extra degree of freedom. As one of the most potentially important perovskite ferroelectrics, lead titanate (PT) is gaining much attentions due to its excellent properties such as high dielectric constant for large charge storage, low fatigue<sup>1,2</sup> etc. It is used for many devices such as microwave, electrooptic device, dynamic random access memories (DRAM), non volatile random access memories (NVRAM)<sup>3,4</sup> etc. As it has a high dielectric constant, PT-based ceramics is very important to reduce its high tetragonality

\*Presented at CONIAPS XI, University of Allahabad, Feb. 20-22, 2010.

and maintain the optimal piezoelectric characteristics for practical applications. Several papers have been reported that the particle size has an important effect tailoring physical properties of the material. It has been observed that the tetragonality ( $c/a$  ratio) of lead based materials can be reduced by particle size. Keeping this in my mind, a novel mechanical activation analysis technique (high-energy ball-milling) has been used to synthesize nanoparticles. Ferroelectric properties of lead titanate are controlled by a suitable substitution at the A site and/or B site, due to the fact that the substitutes may mediate the concentration of the intrinsic defects<sup>5-11</sup>. By the partial substitution of rare earth element such as La in PT the electromechanical anisotropy is conserved<sup>12</sup>. These characteristics make the ceramics suitable for high frequency devices with better performance. The introduction of La elements into the PT perovskite structure ( $ABO_3$ ) produces one lead vacancy for every two La ions. These defects locally break the translational periodicity of the lattice, and then the long-range interaction between ferroelectrically active octahedra containing B-site cations is affected. It is well-known that 3d transition elements in ferroelectric materials with perovskite structure reveal interesting magnetoelectric effects. This approach remains valid in the search for new multiferroic materials suitable for device applications. In view of this, our work has been focused on Mn substitution for the Ti in  $PbTiO_3$  ferroelectric host media. On the other hand, by Mn substitution at the B site the tetragonal distortion can be reduced and also it provides an optimum electromechanical anisotropy. In the present study we report thermal, structural, microstructural and dielectrical properties of doubly doped ( $La^{3+}/Mn^{4+}$ ) lead titanate.

## 2. Experimental Details

Lanthanum ( $La^{+3}$ ) and manganese ( $Mn^{+4}$ ) modified lead titanate (PLMT) nanoceramics with a general formula  $Pb_{0.94}La_{0.06}Mn_xTi_{1-x}O_3$  ( $x = 0.0, 0.04, 0.07, 0.10$ ) were synthesized from high purity ( $\geq 99.9\%$ ) oxides; PbO (with 5 wt % excess) (M/s B.D.H Chemicals),  $La_2O_3$  (M/s Loba Chemie. co. India),  $TiO_2$  (M/s S.D fine Chemicals Ltd.), and  $MnO_2$  (M/s Loba Chemie.co.India) by a high-energy ball-milling technique followed by a solid-state reaction method. The milling was carried out in a Fritsch Pul-verisette P5 planetary ball mill at room temperature for different milling times (10, 20, 30, 40 and 50 h). Milling was carried out in toluene medium (toluene is chemically inert and can be used to diffuse heat that is generated during milling) with (i) WC (tungsten carbide) and milling media (ii) speed of 300 rpm and (iii) ball to powder weight ratio of 10:1, (iv) the milling stopped for 30 minutes after every 1 h of milling to cool down the system. The air-dried powders were heat-treated using thermal gravimetric analyzer (Perkin-Elmer thermal

analyzer (model: diamond) (TGA) to obtain the calcination temperature (at a heating rate of 10 °C /min in argon atmosphere from room temperature up to 1200 °C). Then the powders were calcined at optimized temperature (600 °C) and time (6 h) (based on thermal analyzer and repeated calcinations process) in a programmable furnace with an accuracy of  $\pm 1$  °C. The formation of single phase compounds was confirmed by highly resolved X-ray diffraction data collected by Rigaku Miniflex with CuK $\alpha$  radiation ( $\lambda=1.5418\text{\AA}$ ) in a wide range of Bragg's angles  $2\theta$  ( $20^\circ \leq 2\theta \leq 80^\circ$ ) with scanning rate of 4 °/minute. The calcined powders were used to make cylindrical pellets of diameter 5 mm and thickness 1-2 mm using a hydraulic press at a pressure of  $6 \times 10^7$  N/m<sup>2</sup>. Polyvinyl alcohol (PVC) was used as a binder to prepare the pellets. These pellets were sintered at the optimized temperature (1000 °C) for 2 h in an air atmosphere. The field effect scanning electron micrographs and energy dispersive X-ray analysis (EDAX) are recorded (CARL ZEISS SUPRA 40) to study the surface morphology/ microstructure and chemical composition of the PLMT sintered pellets. The pellet samples were gold coated prior to being scanned under high-resolution field emission gun of FESEM. The gold coating was carried out under argon (Ar) atmosphere. In order to study the electrical properties, both flat surfaces of the samples were polished and electroded with high purity silver paint, and then dried at 150 °C in oven for 3 to 4 h to remove moistures. The electrical measurements were carried out at an input signal level of 1.5 V in a wide temperature range of (35-500 °C) using a computer-controlled impedance analyzer, HIOKI LCR meter, (Model: 3532) in the frequency range of 1 kHz to 1 MHz. The pellets were sintered at 1000 °C for 2 h in an air atmosphere. The measured density of the sintered PLMT pellets was found to be within 97-98 % of its theoretical density.

## 2.1 Thermal Analysis

Thermal gravimetric analysis (TGA) is a useful technique in which a change in weight of a material is recorded as a function of time and temperature. The phase formation of PLMT ceramics was studied using TG analysis. Figure 1 shows the TG thermogram. The weight change occurs in different temperatures regimes: two prominent weight losses are evident, the first one from room temperature to 120 °C is related to the evaporation of free water and the second weight loss with stepwise features occurs upto 500 °C accompanied by a small exothermal feature. It could be related to the lead loss. On the basis of this observation, we can conclude that crystallization of all powders takes place almost at 400 °C, and perovskite structure was established above this temperature<sup>13</sup>. Further increase in the temperature or

in the heating time will only improve the perovskite crystallization because TG curves are not showing weight loss above this temperature.

## 2.2 Phase Analysis

The diffractogram of all ceramics samples showed well crystalline product even at temperature as low as 600 °C (Figure 2). The peaks were indexed using least-squares refinement method and were found to be in accordance with the standard spectrum of JCPDS. All the lattice parameters (given in Table 1) were determined in various crystal systems using a computer program “POWDMULT”<sup>14</sup>. The best agreement between observed (obs) and calculated (cal) interplanar spacing  $d$  (i.e.,  $\sum d_{\text{obs}} - \sum d_{\text{cal}} = \text{minimum}$ ) was found in the tetragonal crystal system like that of the parent compound. The crystalline domain size calculation was performed for the major diffraction peaks using Sherrer equation;  $P_{\text{hkl}} = 0.89\lambda/\beta_{1/2}\cos\theta$ <sup>15,16</sup>, where  $\lambda$  is the wavelength of X-ray (1.5404Å) for CuK $\alpha$  radiation and  $\beta$  is full width at half maxima. Since the ionic radius of Mn<sup>4+</sup> is smaller than that of Ti<sup>4+</sup>, the tetragonality ( $c/a$ ) and unit cell volume decrease on increase of Mn content in PLMT. It has also been found that reduction in particle size is also responsible for the decrement in  $c/a$  ratio as well as in Curie temperature<sup>18</sup>. The change in peak position and intensity is observed because of the change in concentration of Mn. The FESEM images were taken in order to study the surface and crystallite size of the materials. The representative images of all the samples are presented in Figure 3. A highly dense microstructure is obtained with a decrease in grain size on increase substituting of the value of  $x$ . It is suggested that some of the Mn ions segregated at the grain boundaries thereby inhibiting the grain growth.

## 2.3 Dielectric properties

The polycrystalline samples of PLMT ceramics consist of grain, grain boundaries, bulk-electrode interfaces and spread of defects, such as lead and oxygen vacancies. The dielectric dispersion can arise due to domain wall fluctuations, hopping conduction and/or space charge effects. Figure 4 (a&b) shows variation of dielectric constant and dielectric loss with frequency. It is seen in the Figure that above 400 °C, a sudden nonlinearity was found to increase with increase of temperature. This kind of behaviour could be associated to the pure Debye type of relaxation. The higher values of dielectric constant and tangent loss at low frequencies, and higher temperatures could be due to contribution of space charge polarizations to total dielectric response which is reduced slowly with the increase of frequency. The strong dispersion at higher temperature is due to the dc component of dielectric response. The contribution of space charge

polarization is reduced with the increase of frequency. The space charge due to dipole does not response at higher frequencies. Figure 5 shows the dielectric constant variation with respect to temperature at three different frequencies (1 kHz, 10 kHz, and 50 kHz). All the samples show well-defined ferroelectric behaviour. Lead titanate is known to have transition temperature ( $T_c$ ) at 490 °C. Here it has been observed that  $T_c$  decreases with increase in La as well as Mn contents. The lowering of  $T_c$  can be attributed to the decrement in tetragonality ( $c/a$ ) caused by substituents, As they reduce the internal stress, the transition temperature is reduced<sup>17</sup>. The stability of long range interaction of lead titanate type materials is believed to be suppressed by decoupling effects which is caused by the accommodation of ions at the A site of the perovskite structure<sup>18</sup>. Therefore a significant decrement has been observed in  $T_c$  on lanthanum substitution at the A site of the lead titanate while a little variation in  $T_c$  occurred by manganese incorporation at the B site. Further, the transition temperature is found to be almost same for different frequencies. It indicates that all the samples belong to normal ferroelectrics. Figure 6 shows temperature dependency of tangent loss for  $x=0.0$ , dissipation factor does not show a clear anomaly while a peak has been observed near about Curie temperature for the rest samples. This indicates that some thermal process occurring in the material due to maximum energy loss. Above the transition temperature in the paraelectric phase a sharp increase of the dielectric loss is a representative of thermally activated mechanism and can be attributed to loss of oxygen (vacancies) occurring during sintering at high temperature<sup>19</sup>.

#### 2.4 Conductivity Analysis

The variation of ac conductivity ( $\sigma_{ac}$ ) with frequency at different temperatures is shown in Figure 7. For  $x=0.0$  and 0.10 samples, the  $\sigma_{ac}$  presents a dispersion that shifts to higher frequency on increasing temperature and it monotonously decreases with decreasing frequency and saturates at low frequencies. This feature may attribute to the development of a low localization conduction mechanism. The  $\sigma_{ac}$  becomes frequency independent at low frequency (i.e., extrapolation of these curves at low frequencies gives the dc conductivity ( $\sigma_{dc}$ )). The plateau region followed by frequency dispersive region obeys Jonscher's power law. But for  $x = 0.04$  and 0.07 samples as, there are two separate dispersion regions. A low frequency low plateau region which is dominated by the intergranular impedances is followed by conductivity dispersion. Then second plateau region corresponds to the bulk conductivity, and second conductivity dispersion is due to bulk relaxations. The value of hopping frequencies is observed to increase with rise of temperature for all the samples. It suggests

a possible enhancement in the carrier-hopping rate of the mobile charge carriers with rise in temperature. The deviation from low frequency plateau at lower temperatures may be assigned to electron conduction through quantum-mechanical tunneling between localized states. Thermal behavior of ac conductivity of all the samples is shown in Figure 8. The Curie temperature obtained from ac conductivity measurements is in full agreement with the  $T_c$  values found from the temperature dependency of the dielectric constant of PLMT ceramics. It is seen that the conductivity is found to increase with increase in temperature. The change in slope of curve will reflect a change in the conductivity phenomenon in para and ferroelectric regions. The value of activation energy was calculated from the slope of the graphs of the conductivity is given in Table 1. It is obvious that in the low temperature region, the ac conductivity depends significantly on the frequency, which was observed in this type of materials<sup>20</sup>. At lower temperatures and higher frequencies it is observed to be independent of temperature. However, with the increase in temperature the dielectric relaxation takes place and the dependency of the conductivity on frequency gets reduced. Figure 9 shows the variation of dc conductivity ( $\sigma_{dc}$ ) with inverse of absolute temperature of all the samples. The temperature variation of conductivity is an important means to judge the applicability of the compounds for devices. The bulk resistance  $R_b$  of samples from the data fitting of complex impedance plots on the basis of proposed equivalent circuit was derived. The dc conductivity is calculated from the bulk

resistance  $R_b$ , using the formula;  $\sigma_{dc} = \frac{l}{R_b A}$ , where  $l$  is the thickness of the

sample and  $A$  is the area of the electrode deposited on the sample. The dc conductivity increases with rise in temperature. The nature of variation of  $\sigma_{dc}$  appears to be of Arrhenius type in different range of temperature. The linear variation of  $\sigma_{dc}$  is governed by the relation  $\sigma = \sigma_0 e^{E_a/kT}$  where  $E_a$  is the activation energy and  $k$  is the Boltzman's constant. It is observed that the dc conductivity increases with increase in temperature for all the compounds. This suggests that these compounds have negative temperature coefficient of resistance (NTCR) at higher temperature. Due to the variable valence states of Mn with their random and disorder distribution at the B-site of the lead based perovskite, different 3d metal-oxygen vacancy complexes may be produced. This eventually results in a short range hopping of oxygen ions. Activation energies (given in Table 1) calculated from the dc part of ac conductivity vs temperature plots and dc conductivity vs temperature plots were found almost similar.

### 3. Conclusions

A mechanical activation (high energy ball milling) followed by some heat treatment has been used to prepare nanocrystalline powder of PLMT ceramics. Preliminary structural technique (HRXRD) shows the formation of material. All samples show a non-relaxor type of phase transition. The results also indicate that the crystallite size plays an important role in deciding the dielectric parameters. A universal power law relation was brought into picture to explain the frequency dependence of ac conductivity. The temperature dependence of ac conductivity was analyzed in details. The activation energy obtained from the temperature dependence of ac conductivity graphs was attributed to the shallow trap-controlled space charge conduction in the bulk of the sample.

Table 1. Lattice parameters, crystalline size, grain size and activation energies (dc and ac conductivity in eV) of  $\text{Pb}_{0.92}\text{La}_{0.08}\text{Mn}_x\text{Ti}_{1-x}\text{O}_3$  ( $x = 0.0, 0.04, 0.07, 0.10$ ) compounds

x	a(Å)	c(Å)	(c/a) ratio	P (nm)	Dielectric constant	Average grain size (nm)	E <sub>dc</sub>	E <sub>ac</sub>
0.0	3.898	4.152	1.06	11.54	2043	860	1.12	1.14
0.04	3.895	4.073	1.04	14.68	7590	700	0.62	0.64
0.07	3.903	4.083	1.04	13.61	5587	675	0.60	0.59
0.10	3.905	4.066	1.04	11.31	14799	525	0.36	0.48

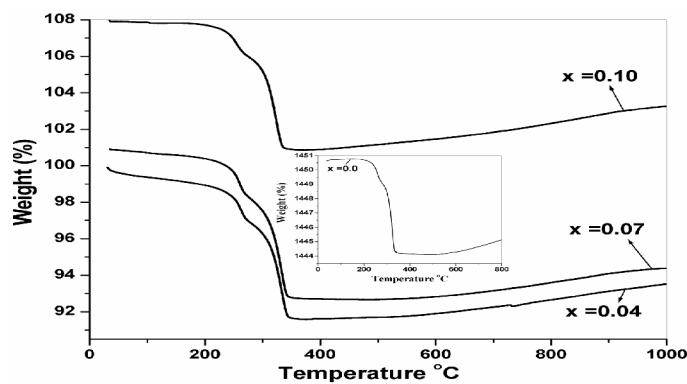


Figure 1  
TGA pattern of PLMT ( $x = 0.0, 0.04, 0.07, 0.10$ ) compounds.

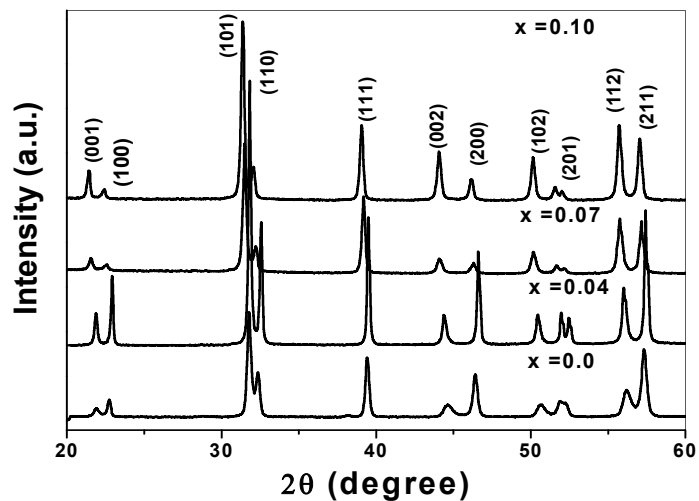


Figure 2

Room temperature HRXRD pattern of PLMT ( $x = 0.0, 0.04, 0.07, 0.10$ ) compounds.

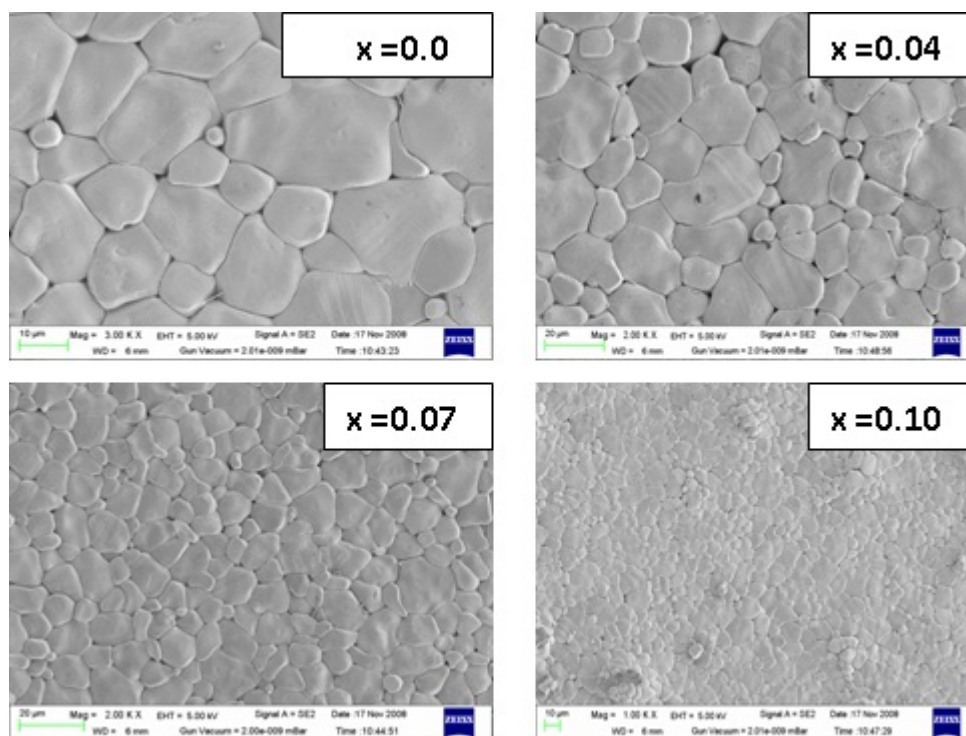


Figure 3. Field emission scanning electron micrographs (FESEM) of PLMT ( $x = 0.0, 0.04, 0.07, 0.10$ ) compounds.

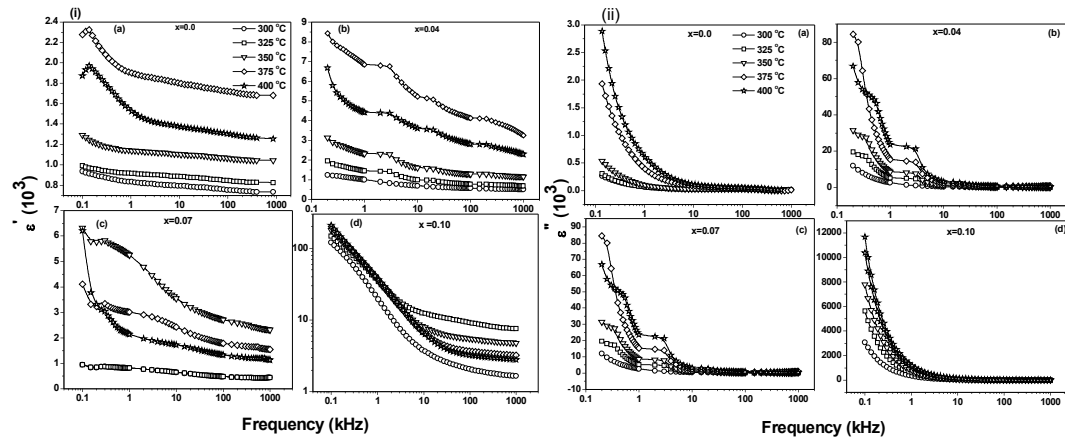


Figure 4. (a) Variation of dielectric constant with frequency of PLMT ( $x = 0.0, 0.04, 0.07, 0.10$ ) compounds at room temperature (b) Variation of dielectric loss with frequency of PLMT ( $x = 0.0, 0.04, 0.07, 0.10$ ) compounds at different temperatures.

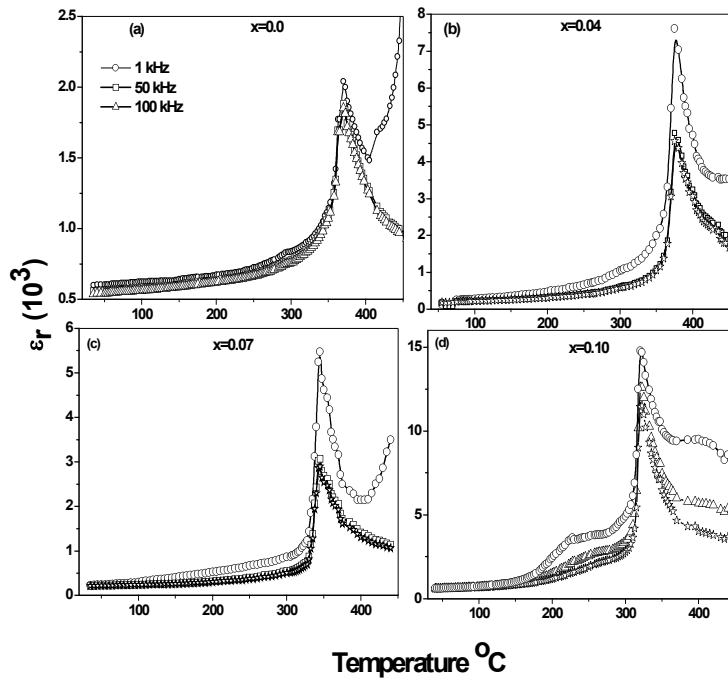


Figure 5

Variation of dielectric constant of PLMT ( $x = 0.0, 0.04, 0.07, 0.10$ ) compounds with temperature at 1, 10 and 50 kHz frequency.

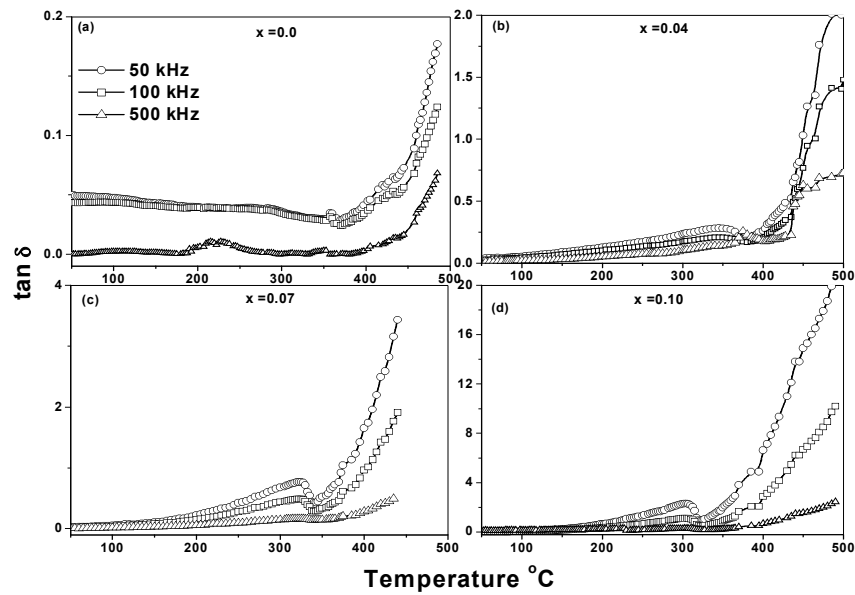


Figure 6

Variation of dielectric loss of PLMT ( $x = 0.0, 0.04, 0.07, 0.10$ ) with temperature at 10, 50 and 100 kHz frequency.

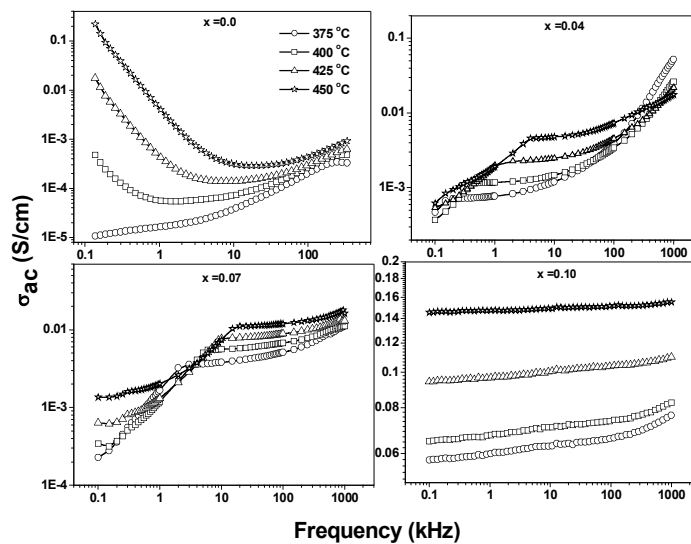


Figure 7

Variation of ac conductivity as a function of frequency for PLMT ( $x = 0.0, 0.04, 0.07, 0.10$ ) compounds.

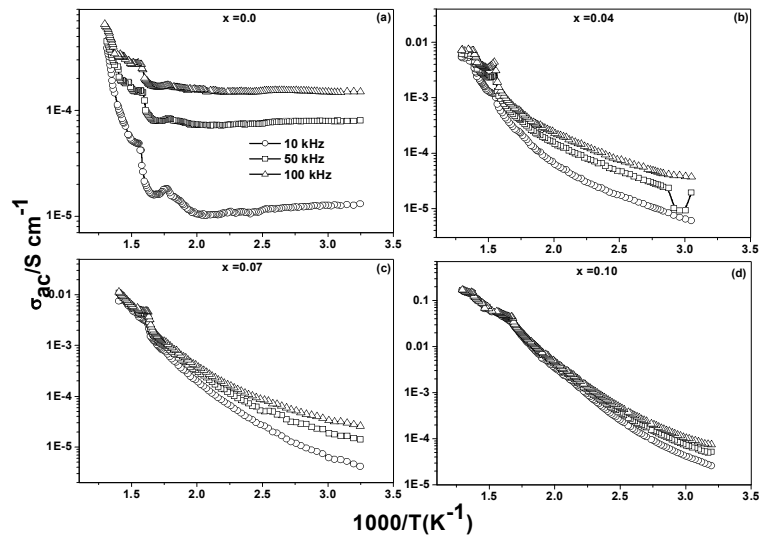


Figure 8

Variation of ac conductivity as a function of temperature for PLMT ( $x = 0.0, 0.04, 0.07, 0.10$ ) compounds.

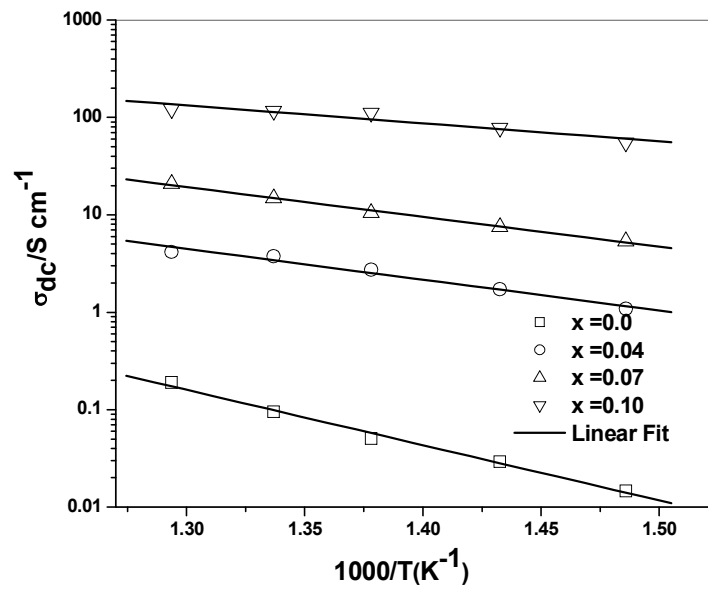


Figure 9

Arrhenius plot of dc conductivity of PLMT ( $x = 0.0, 0.04, 0.07, 0.10$ ) compounds.

### References

1. A. J. Moulson and J. M. Herbert, *Electroceramics (2nd ed.)*, Wiley, Chichester, 2003.
2. B. Jaffe, W. R. Cook and H. Jaffe, *Piezoelectric Ceramics*, Academic Press, New York, 1971.
3. O. Bouquin, M. Lejeune and J. P. Boilot, *J. Am. Ceram. Soc.*, **74** (1991)1152-1156.
4. T. R. Gururaja, A. Safari and A. Halliyal, *Am. Ceram. Soc. Bull.*, **65** (1986)1601-1603.
5. M. V. Raymond, J. Chen, and D. M. Smyth, *Integr. Ferroelectr.*, **5** (1994) 73-78.
6. Q. Y. Jiang, E. C. Subbarao, and L. E. Cross, *J. Appl. Phys.*, **75** (1994) 7433-7443.
7. K. Miura and M. Tanaka, *Jpn. J. Appl. Phys.*, **35** (1) (1996) 3488-349.
8. S. B. Majumder, Y. N. Mohapatra, and D. C. Agrawal, *Appl. Phys. Lett.*, **70**(1997)138-140.
9. T. Kijima, T. Aoyama, H. Miyazawa, Y. Hamada, K. Ohashi, M. Nakayama, E. Natori, and T. Shimoda, *Jpn. J. Appl. Phys.*, **44** (1) (2005) 267-274.
10. S. Shannigrahi and K. Yao, *Appl. Phys. Lett.*, **86** (2005) 092901-3.
11. O. P. Martinez, F. Calderon, A. Penton, E. Suaste, M. Rivera, F. Leccabue, G. Boccelli and E Watts, *Rev Mex Fis.*, **41** (1995) 85-94.
12. M. Dawber, J. F. Scott, and A. J. Hartmann, *J. Eur. Ceram. Soc.*, **21** (2001) 1633-1636
13. R. Thomas, S. Mochizuki, T. Mihara and T. Ishida, *Thin Solid Films*, **443** (2003) 14-22.
14. POWD MULT: an interactive powder diffraction data interpretation and indexing Programs v 2.1, E.Wu School of Physical science, Hindess university of South Australia, Bedford Park, SA 5042, Australia
15. H. P. Klung, L. B. Alexander, *X-ray Diffraction Procedures, 2nd edn.* (Wiles, New York), (1974) 687-89.
16. B. D. Cullity, *Elements of X-Ray Diffraction* (Philippines: Addison-Wesley) (1978) 278-284.
17. K. Okazaki, *Am. Cerm. Soc. Bull.*, **63** (1984) 1150-1157
18. A. Pelaiz-Barranco, Y Gonzalez Abreu and R Lopez-Noda, *J. Phys: Condense Matter*, **20** (2008) 505208-505218.
19. S. Ananta and N.W. Thomas, *J. Eur. Ceram. Soc.*, **19** (1999) 629-635.
20. K. S. Rao, P. M. Krishna, T. S. Latha and D. M. Prasad, *Mat Sci and Engg.*, **131** (B) (2006) 127-131.